

# Seismic retrofitting by base-isolation of r.c. framed buildings exposed to different fire scenarios

Fabio Mazza\* and Mirko Mazza<sup>a</sup>

*Dipartimento di Ingegneria Civile, Università della Calabria 87036 Rende (Cosenza), Italy*

*(Received August 12, 2017, Revised October 1, 2017, Accepted October 3, 2017)*

**Abstract.** Base-isolation is now being adopted as a retrofitting strategy to improve seismic behaviour of reinforced concrete (r.c.) framed structures subjected to far-fault earthquakes. However, the increase in deformability of a base-isolated framed building may lead to amplification in the structural response under the long-duration horizontal pulses of high-magnitude near-fault earthquakes, which can become critical once the strength level of a fire-weakened r.c. superstructure is reduced. The aim of the present work is to investigate the nonlinear seismic response of fire-damaged r.c. framed structures retrofitted by base-isolation. For this purpose, a five-storey r.c. framed building primarily designed (as fixed-base) in compliance with a former Italian seismic code for a medium-risk zone, is to be retrofitted by the insertion of elastomeric bearings to meet the requirements of the current Italian code in a high-risk seismic zone. The nonlinear seismic response of the original (fixed-base) and retrofitted (base-isolated) test structures in a no fire situation are compared with those in the event of fire in the superstructure, where parametric temperature-time curves are defined at the first level, the first two and the upper levels. A lumped plasticity model describes the inelastic behaviour of the fire-damaged r.c. frame members, while a nonlinear force-displacement law is adopted for the elastomeric bearings. The average root-mean-square deviation of the observed spectrum from the target design spectrum together with a suitable intensity measure are chosen to select and scale near- and far-fault earthquakes on the basis of the design hypotheses adopted.

**Keywords:** seismic retrofitting; r.c. framed buildings; base-isolation system; fire scenarios; spectral matching; nonlinear dynamic analysis

## 1. Introduction

Significant degradation of reinforced concrete (r.c.) framed structures occurs during a fire, with decline of compressive strength and modulus of elasticity for the concrete and yield strength for the steel reinforcement (Youssef and Mofteh 2007). Note that residual mechanical properties of the concrete after fire can be lower or higher than those occurring during exposure to fire, depending on the maximum fire temperature and the heating and cooling rates (Lee *et al.* 2008). In addition, increased susceptibility to explosive spalling, due to a sudden break up of concrete on the sides of structural elements exposed to fire, is observed for high-strength concrete, while spalling does not usually occur in r.c. frame members made with normal-strength concrete (Dwaikat and Kodur 2009). On the other hand, the type of steel and maximum temperature during a fire have a significant effect on post-fire properties of the reinforcing bars, with carbon-steel bars recovering most of their initial values after cooling provided the temperature stayed below a critical threshold (Felicetti *et al.* 2009). Since an overall amplification of the post-fire seismic

vulnerability of r.c. framed structures is expected, even if total collapse as a result of fire occurs rarely, the question to be answered in this work is whether the post-fire ultimate seismic safety level can be increased by using a base-isolation system.

Aftershocks following fire may find seismic load capacity of r.c. structures notably reduced vis-à-vis the no-fire condition, with an amplification in the structural response localized to the level of the fire compartment. Specifically, thermal analysis (Mazza 2015a) and experimental results (Mostafei 2013a, b) have highlighted: i) notable decrease of stiffness in the structural members exposed to fire; ii) marked narrowing of the axial load and bending moment interaction domain of columns exposed to fire on all sides (e.g., interior columns), especially for values of the compressive axial load greater than the balanced value; iii) significant decrease in flexural strength on the bottom side of the beams exposed to fire on three sides (e.g., interior beams); iv) decrease in ductility on the top side of interior beams, through damage to the compression zone of concrete and the corresponding longitudinal reinforcement. In recent years, many authors have dealt with seismic retrofitting techniques, following different approaches (Gilmore 2012, Foti 2015, Mazza 2015b, Sorace and Terenzi 2014, 2015, Tavakoli *et al.* 2015, Zerbin and Aprile 2015). Among these, base-isolation shifts the fundamental frequency of the structure away from the dominant frequencies of far-fault earthquakes, but the long-duration (horizontal) directivity and fling-step pulses in a

\*Corresponding author, Professor

E-mail: [fabio.mazza@unical.it](mailto:fabio.mazza@unical.it)

<sup>a</sup>Ph.D.

E-mail: [mirko.mazza@unical.it](mailto:mirko.mazza@unical.it)

near-fault area can become critical for base-isolated r.c. framed structures if the pulse intensity is so strong that the superstructure undergoes plastic deformations (Mazza and Vulcano 2012). This problem may be amplified in fire-weakened base-isolated r.c. framed structures.

In order to evaluate the effectiveness of base-isolation in the retrofitting of fire-damaged r.c. framed structures, the nonlinear seismic response of retrofitted structural systems is compared with that of the corresponding original structures without any retrofit. To this end, a five-storey r.c. office building is initially designed as fixed-base in line with a former Italian seismic code (DM96 1996) and a medium-risk zone is selected. Five fire scenarios are simulated assuming the fire compartment is confined to the area of the first level (i.e., F1), the first two (i.e., F1/2) and the upper (i.e., Fi,  $i=3-5$ ) levels of the superstructure. Parametric temperature-time fire curves are determined based on Eurocode 1 (EC1 2004), and reduced mechanical properties of r.c. cross-sections of beams and columns are assumed in accordance with the 500°C isotherm provided by Eurocode 2 (EC2 2004) considering 60 (i.e., R60) minutes of resistance. Then, the fire-damaged test structures are retrofitted by the insertion of high-damping-laminated rubber bearings (HDLRBs) to meet the requirements of the current Italian code (NTC08 2008) in a high-risk seismic zone. A comparison of the nonlinear dynamic analysis for the original (fixed-base) and retrofitted (base-isolated) framed structures, before (i.e., FB and BI) and after (i.e., FB.Fi and BL.Fi) fire exposure, is carried out. Near-fault (i.e., NFE) and far-fault (i.e., FFE) sets of earthquakes are selected, minimizing the scale factors and the root mean square deviation from the target design spectrum of the test structures (Bommer and Acevedo 2004).

## 2. Original and retrofitted test structures in the no-fire condition

A five-storey office building regular in plan (Fig. 1(a)) and in elevation (Fig. 1(b)) is considered as test structure for the original (i.e., fixed-base, FB) configuration. For the sake of simplicity, the plane frames orientated along the horizontal ground motion direction perpendicular to the floor slab direction (Y) are considered as reference scheme

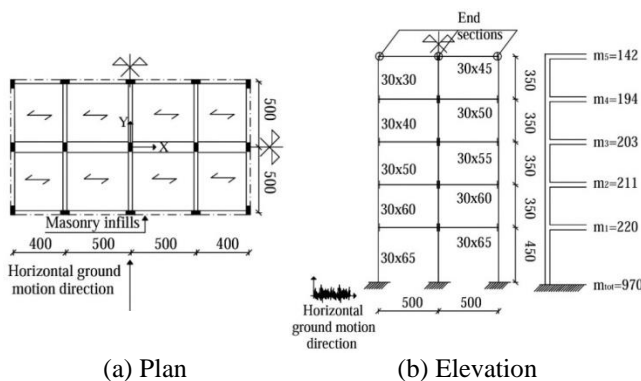


Fig. 1 Original (fixed-base) r.c. test structure in the no-fire condition (units in cm and ton)

(Fig. 1(a)).

Dead and live gravity loads used in the design are assumed equal to: 4.48 kN/m<sup>2</sup> and 3 kN/m<sup>2</sup>, for the top floor, and 5.18 kN/m<sup>2</sup> and 3 kN/m<sup>2</sup>, for the other floors, of the FB structure. Masonry infills are taken into account by considering a gravity load of 2.7 kN/m<sup>2</sup> along the perimeter. Seismic loads are evaluated in line with the former Italian seismic code (DM96 1996), assuming: medium-risk seismic region (degree of seismicity  $S=9$ , which corresponds to a coefficient of seismic intensity  $C=0.07$ ) and a medium subsoil class (subsoil parameter  $S=1$ ); cylindrical compressive strength equal to 25 N/mm<sup>2</sup> for the concrete and a yield strength of 450 N/mm<sup>2</sup> for the steel. Floor masses and cross-sections of the r.c. frame members, also reported in Fig. 1(b), correspond to a fundamental vibration period  $T_{1Y,FB}=0.749$  s and an effective mass  $m_{1,X}=0.804 m_{tot}$ . Further details regarding the design of the test structure can be found in Mazza (2015a).

To retrofit the original (fixed-base) framed building, to meet performance levels imposed by the current Italian code (NTC08 2008) in a high-risk seismic zone (peak ground acceleration on rock,  $a_g=0.351$  g at the collapse prevention limit state) and medium subsoil class (class C, site amplification factor  $S=1.179$ ), HDLRBs with same dimensions, so as to increase torsional stiffness of the base-isolation system, are installed below all columns of the original structure (Fig. 2). An additional mass of 286 tons is considered above the isolation level, at the level of the existing foundation, while a new foundation is hypothesized on the assumption that it would be possible to temporarily jack up the whole structure. The design of the base-isolation system is carried out on the assumption that the fundamental vibration period of the retrofitted structure (i.e., base-isolated, BI) satisfies the condition  $T_{1Y,BI}(=2.5$  s)  $\geq 3T_{1Y,FB}$  and considering equivalent viscous damping ratios  $\chi_H=10\%$  and  $\chi_V=5\%$  in the horizontal and vertical directions, respectively. A nominal stiffness ratio  $\alpha_{K0}$ , defined as the ratio between the nominal value of the vertical stiffness ( $K_{V0}$ ) and the analogous value of the horizontal stiffness ( $K_{H0}$ ), equal to 1200 is assumed for all the isolators, considering a volumetric compression modulus of the rubber  $E_b=2000$  MPa and a shear modulus  $G=0.40$  MPa. The design of the HDLRBs fulfill the CP limit state checks: i.e.,  $\gamma_{tot} \leq 5$  and  $\gamma_s \leq 2$ , where  $\gamma_{tot}$  represents

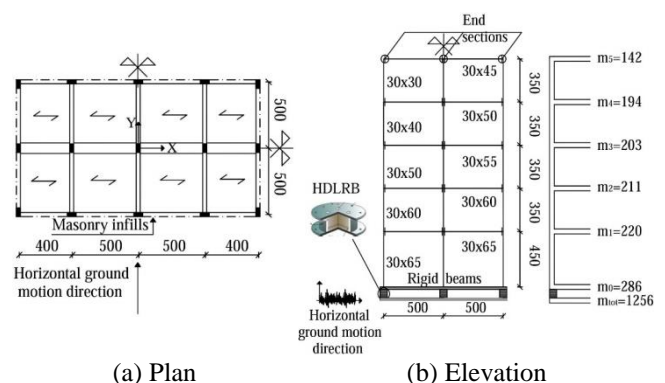


Fig. 2 Original (base-isolated) r.c. test structure in the no-fire condition (units in cm and ton)

Table 1 Design parameters of the HDLRBs (units in kN, cm and s)

$K_{H0}$	$K_{V0}$	$C_H$	$C_V$	$D_s$	$D_e$	$t_e$	$S_1$	$S_2$	$E_c$	$\gamma_s$	$\gamma_{tot}$	$(P_{cr}/P)_{min}$
5.18	6220	0.41	2.9	65	61	26	19.2	2.4	55.12	0.93	1.77	2.00

the total design shear strain, while  $\gamma_s$  represents the shear strain of the elastomer due to seismic displacement;  $(P_{cr}/P)_{min} \geq 2$ , where  $P$  and  $P_{cr}$  represent the maximum compression axial load and the corresponding critical buckling load. Further details regarding the design of the base-isolation system can be found in Mazza and Vulcano (2012).

In Table 1 (initial) horizontal and vertical stiffnesses (i.e.,  $K_{H0}$  and  $K_{V0}$ ) and corresponding equivalent damping coefficients  $C_H (\approx \chi_H K_{H0} T_{IH} / \rho)$  and  $C_V (\approx \chi_V K_{V0} T_{IV} / \rho)$  of the HDLRBs, are reported together with the following geometrical properties: diameter of the steel layer ( $D_s$ ) and that of the elastomer ( $D_e$ ); total thickness of elastomer ( $t_e$ ); primary ( $S_1$ ) and secondary ( $S_2$ ) shape factors; compression modulus ( $E_c$ ). The results of the verifications for the isolators are also reported in Table 1. It should be noted that the design of the isolators depends on the condition imposed on the minimum value of  $(P_{cr}/P)$ , while no tensile forces are found in the isolators.

### 3. Original and retrofitted test structures in the fire-damaged scenarios

Five fire scenarios are considered for the original (i.e., fixed-base with fire, FB.F in Fig. 3) and retrofitted (i.e., base-isolated with fire, BI.F in Fig. 4) test structures, assuming the fire compartment is confined to the area of the first level (i.e., F1), the first two (i.e., F1/2, with F1 and F2 occurring simultaneously) and the upper (i.e., Fi,  $i=3-5$ ) levels. The interior beams and columns are exposed to fire on three and four sides, respectively, while all exterior frame members are exposed on one side (Figs. 3(a) and 4(a)).

An opening factor is evaluated to represent the amount of ventilation (EC1 2004)

$$O = A_v h_{eq}^{0.5} / A_t \quad (1)$$

as function of the total area of enclosure ( $A_t$ ), the total area of vertical openings ( $A_v$ ) and the weighted average height of windows ( $h_{eq}$ ). Then, a thermal absorptivity coefficient of the fire compartment is considered

$$b = \sum_j (b_j \cdot A_j) / (A_t - A_v) \quad (2)$$

$b_j$  and  $A_j$  being the absorptivity coefficient and area of the  $j$ -th enclosure surface (i.e., masonry infills, top and bottom floor slabs). Finally, the fire load density

$$q_{t,d} = Q_{f,k} \cdot \delta_{q2} \cdot \delta_n / A_t \quad (3)$$

is related to the characteristic fire load ( $Q_{f,k}$ ), where:  $\delta_{q1}$  and  $\delta_{q2}$  are dimensionless factors, taking into account the fire

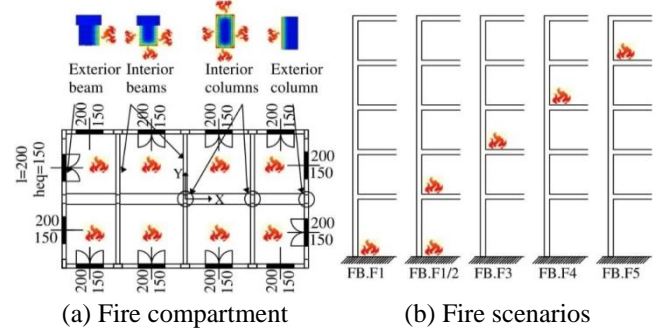


Fig. 3 Original (fixed-base) r.c. test structure in the fire-damaged conditions (units in cm)

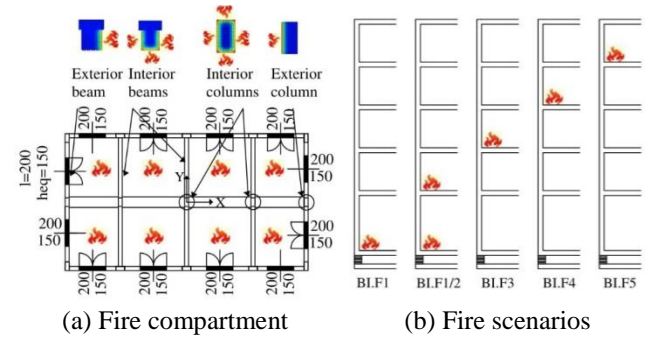


Fig. 4 Retrofitted (base-isolated) r.c. test structure in the fire-damaged conditions (units in cm)

Table 2 Design parameters of the fire load (R60 fire resistance)

Fire compartment	$A_t$ [m <sup>2</sup> ]	$A_v$ [m <sup>2</sup> ]	$h_{eq}$ [m]	$O$ [m <sup>0.5</sup> ]	$b$ [J/m <sup>2</sup> s <sup>1/2</sup> K]	$q_{fd}$ [MJ/m <sup>2</sup> ]	$Q_{f,k}$ [MJ]	$\delta_{q1}$	$\delta_{q2}$	$\delta_n$
First level	612	24	1.5	0.048	1125.8	186.4	114102	1	1	1
Upper levels	556	24	1.5	0.053	1135.8	205.2	114102	1	1	1

risk due to the size of the compartment and the type of occupancy, respectively;  $\delta_n$  is a dimensionless factor to account for the different firefighting measures. In Table 2 the design parameters of the fire load for the first and upper levels of the test structures are reported, with reference to 60 min (i.e., R60) of exposure. Further details on fire modelling can be found in Mazza (2015a).

To simulate the time-temperature evolution, during the heating and cooling phases of an actual fire, the EC1 natural fire curves (EC1, 2004) are considered

$$\theta_g = 20 + 1325 \left( 1 - 0.324e^{-0.2t^*} - 0.204e^{-1.7t^*} - 0.472e^{-19t^*} \right) \quad (4a)$$

$$\theta_g = \theta_{max} - 250 \left( 3 - t_{max}^* \right) \left( t^* - t_{max}^* \right) \quad (4b)$$

where  $t^*$  is a fictitious time obtained by considering the time  $t$  (in hours) multiplied by the opening factor  $O$ , while  $t_{max}^*$  corresponds to the maximum temperature  $\theta_{max}$  in the heating phase

$$t_{max}^* = \left( 0.2 \cdot 10^{-3} q_{t,d} / O \right) \Gamma \quad (5)$$

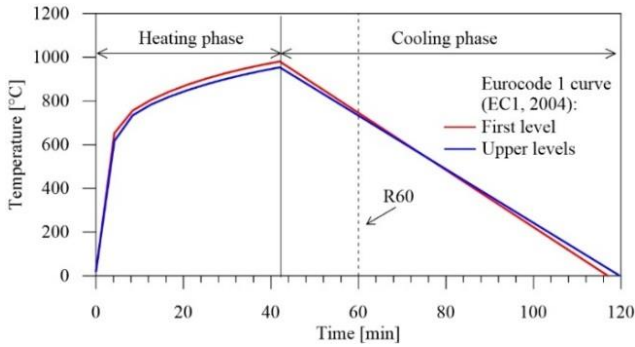


Fig. 5 Natural (EC1) fire curves for different fire scenarios

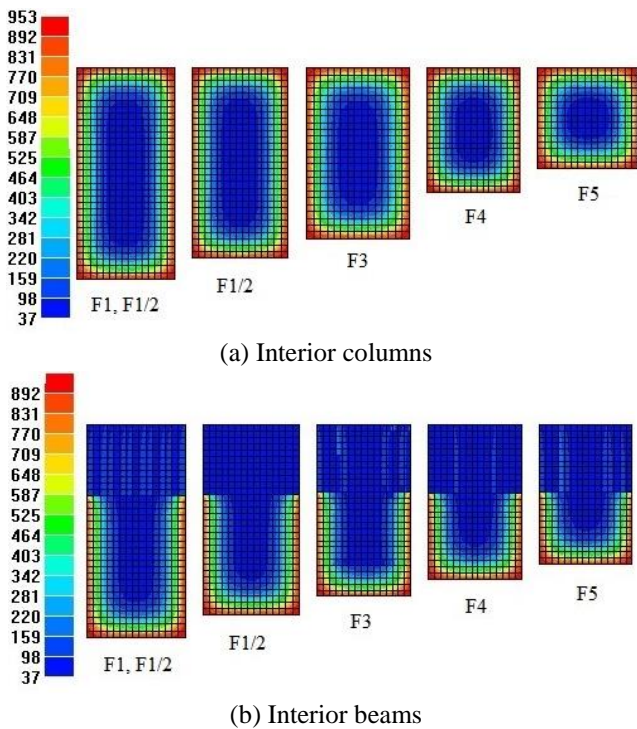


Fig. 6 Thermal mappings of r.c. cross sections for different fire scenarios

as function of the dimensionless parameter

$$\Gamma = (O/b)^2 / (0.04/1160)^2 \quad (6)$$

The corresponding EC1 time-temperature curves are shown in Fig. 5, with reference to the first and upper levels of the superstructure. As can be observed, similar curves are obtained for different fire scenarios while temperatures corresponding to R60 are placed in the cooling branch.

The temperature distribution in the frame members of the test structure at R60 is obtained by means of software for thermal analysis (PROSAP), as function of the EC1 time-temperature curve of the fire compartment. As expected, the increase in temperature is greater in the case of cross-sections exposed on four or three sides, while limited effects are observed for those exposed to fire on one side only. As an example, thermal mappings of the interior columns and beams for different fire scenarios, assuming a direct correspondence between the examined level and the

fire compartment, are plotted in Figs. 6(a) and 6(b), respectively. Then, the residual seismic load capacity of the cross-sections in terms of stiffness, strength and ductility is evaluated in line with the 500°C isotherm method proposed by Eurocode 2 (EC2 2004). In particular, a decrease of flexural stiffness from a minimum of 46% and 37%, for the F1 scenario, to a maximum of 65% and 40%, for the F5 scenario, is obtained for the interior columns and beams, respectively. Moreover, a reduction of about 39%, at the first storey, and 53%, at the fifth storey, of the ultimate domain between axial load and bending moment is observed for the interior columns, especially for values of the compressive axial load greater than those corresponding to the balanced compressive load. On the other hand, a significant decrease in flexural strength is experienced on the bottom side of the interior beams, with a reduction of about 55% (F1 scenario) and 45% (F5 scenario). Finally, ultimate ductility shows a maximum reduction of roughly 30% and 33% for the interior columns and beams, respectively. Further results, omitted for the sake of brevity, can be found in Mazza (2015a).

#### 4. Selection and scaling of near- and far-fault earthquakes

The features of earthquakes recorded in close proximity to the source can be significantly different from those observed for far-fault ground motions (Somerville 1997; Bray *et al.* 2009), highlighting sometimes two-sided velocity pulses without permanent ground displacement (i.e., forward directivity effects) and other times one-sided velocity pulses generating permanent ground displacement (i.e., fling-step effects). Specifically, the arrival of low-frequency pulses at the beginning of velocity and displacement time-histories, whose duration is expected to scale with magnitude (Baltzopoulos *et al.* 2016), may produce the maximum response of the structure in a wave-like behaviour before a resonant mode-like response build up (Iwan 1997). Amplification in the inelastic demand of the superstructure is generally expected for fire-damaged existing fixed-base structures subjected to far-fault earthquakes (Mazza 2015a) and fire-damaged new base-isolated structures subjected to near-fault earthquakes (Mazza 2017). However, additional study is required to evaluate the nonlinear seismic behaviour of fire-damaged r.c. framed structures retrofitted with a base-isolation system and located near or far from active faults. To this end, seven near-fault earthquakes (i.e., NFE set) are selected from the Pacific Earthquake Engineering Research center database. Next, seven far-fault earthquakes (i.e., FFE set), reflecting the provisions of the Italian seismic code (NTC08, 2008) for the geographical coordinates (longitude 16.185° and latitude 39.333°) at the site in question (i.e., subsoil class C), are taken from the European Strong Motion database. In Tables 3 and 4, the main data of the NFE and FFE sets are reported, respectively: country, earthquake, date, recording station, component, magnitude ( $M_w$ ), peak ground acceleration in the horizontal direction ( $PGA_H$ ).

Table 3 Main data of the selected near-fault ground motions (NFE set)

Earthquake	Date	Station	Component	$M_w$	$PGA_H$	$D_{rms}$
Chi-Chi, Taiwan	20/09/1999	TCU068	EW	7.3	0.566 g	0.0304
Northridge, U.S.A.	17/01/1994	Rinaldi	228	6.6	0.837 g	0.0237
Superstition Hills, U.S.A.	24/11/1987	Parachute	225	6.4	0.455 g	0.0559
Cape Mendocino, U.S.A.	25/04/1992	Petrolia	090	7.1	0.662 g	0.0155
Kobe, Japan	16/01/1995	Takatori	090	6.9	0.616 g	0.0544
Tabas, Iran	16/09/1978	Tabas	TR	7.7	0.852 g	0.0220
Erzincan, Turkey	13/03/1992	Erzincan	NS	6.7	0.515 g	0.0289

Table 4 Main data of the selected far-fault ground motions (FFE set)

Earthquake	Date	Station	Component	$M_w$	$PGA_H$	$D_{rms}$
Friuli, Italy	15/09/1976	Forgaria-Cornio	EW	6.0	0.336 g	0.0526
Montenegro	15/04/1979	Bar-Skupstina Opstine	EW	6.9	0.363 g	0.0512
Campano-Lucano, Italy	23/11/1980	Calitri	EW	6.9	0.176 g	0.0408
Kalamata, Greek	13/09/1986	Kalamata-Prefecture	N265	5.9	0.215 g	0.0242
Kalamata, Greek	13/09/1986	Kalamata-Prefecture	N355	5.9	0.297 g	0.0189
Erzincan, Turkey	13/03/1992	Erzincan-M.Mudurlugu	N279	6.6	0.513 g	0.0265
South Iceland, Iceland	17/06/2000	Kaldarholt	LONG	6.5	0.625 g	0.0369

Since acceleration response spectra of real ground motions does not exactly match the target design spectrum, only the NF and FF records whose spectrum matches the specified spectrum to a certain value of the root mean square difference ( $D_{rms}$ ), between a scaled spectrum and a target spectrum, are selected (Bommer and Acevedo 2004)

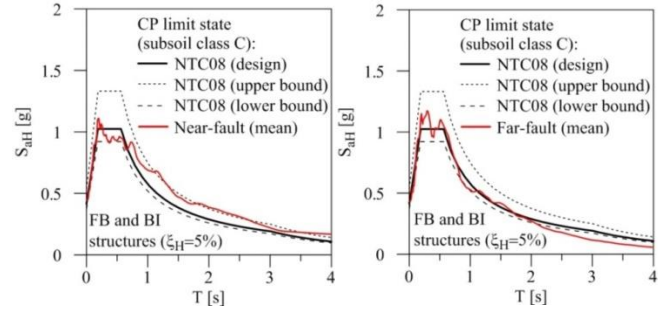
$$D_{rms} = \frac{1}{N} \sqrt{\sum_{i=1}^N \left( \frac{S_a^{real}(T_i)}{PGA_{real}} - \frac{S_a^{NTC08}(T_i)}{PGA_{NTC08}} \right)^2} \quad (7)$$

expressed as function of the normalized spectral ordinate of acceleration at a vibration period  $T_i$  ( $i=1..N$ ) of the NTC08 target (i.e., at the collapse prevention, CP, limit state) and selected real motion,  $N$  being the number of vibration periods used in the calculation. Parameter  $D_{rms}$  supplies a quantitative evaluation of the similarity between the frequency contents of the real and NTC08 spectra: i.e., lower values of  $D_{rms}$  (e.g., less than 0.2) correspond to a closer match between the shape of the selected and target spectra.  $D_{rms}$  values corresponding to the NFE and FFE sets of earthquakes are also reported in Tables 3 and 4, respectively.

The selection of an intensity measure to predict structural demand of fixed-base and base-isolated buildings can be quite tricky, because ground motions characterized by similar spectral values at specific vibration periods can produce different responses as the structure enters the inelastic range and the effects of the higher vibration modes are taken into account. Numerous approaches are to be found in the literature for scaling real accelerograms in order to obtain robust estimates of the structural response (Mollaioli *et al.* 2013; Mazza and Labernarda 2017). In detail, the In-Spector software is adopted in the present study for a computer aided selection of real spectrum-compatible NFE and FFE sets (Acunzo *et al.* 2014). This is combined with the *Modified Acceleration Spectrum Intensity (MASI)* evaluated from integration of spectral values of acceleration ( $S_a$ ) in the range of vibration periods  $T_1-T_2$

Table 5 Scale factors for the NFE and FFE sets at the CP limit state

Earthquake	$SF_{NFE}$	Earthquake	$SF_{FFE}$
Chi-Chi	0.78	Friuli	1.53
Northridge	0.50	Montenegro	1.43
Superstition Hill	0.55	Campano-Lucano	2.94
Cape Mendocino	0.48	Kalamata	1.74
Kobe	0.65	Kalamata	2.15
Tabas	0.48	Erzincan	1.01
Erzincan	0.79	South Iceland	1.01



(a) Near-fault earthquakes (b) Far-fault earthquakes

Fig. 7 Acceleration (elastic) response spectra

$$MASI = \int_{T_1}^{T_2} S_a dT \quad (8)$$

where the lower limit accounts for the contribution of higher modes to structural response while the upper limit considers the lengthening of period due to the nonlinear structural behaviour. As suggested by Mollaioli *et al.* (2013), the integration interval is assigned equal to  $0.2T_{1Y,FB}(=0.15s)$ – $1.5T_{1Y,FB}(=1.125s)$ , for fixed-base structures, and  $0.5T_{1Y,BI}(=1.25s)$ – $1.25T_{1Y,BI}(=3.125s)$ , for base-isolated structures. Then, the selected real NF and FF earthquakes are normalized with respect to the NTC08 ones at the CP limit state, by scaling their  $PGA_H$  values

$$\begin{aligned} PGA_{H, Scaled}^{NFE} &= PGA_H^{NFE} \cdot SF_{NFE} \\ PGA_{H, Scaled}^{FFE} &= PGA_H^{FFE} \cdot SF_{FFE} \end{aligned} \quad (9)$$

through the Scale Factors ( $SFs$ )

$$\begin{aligned} SF_{NFE} &= MASI_{NTC08} / MASI_{NFE} \\ SF_{FFE} &= MASI_{NTC08} / MASI_{FFE} \end{aligned} \quad (10)$$

It should be noted that the NFEs are scaled to the aforementioned interval of vibration periods corresponding to the BI structures, while the FFEs are scaled to the analogous interval for the BF structures, thereby obtaining a reasonable spectral match also for the BF and BI test structures, respectively.

Specifically, the mean response spectrum of the NFE and FFE sets match NTC08 spectrum at any point on the considered range of vibration periods, assuming lower and upper bound tolerances equal to 10% and 30%, respectively. In Table 5 scale factors of the selected NF and FF sets of earthquakes are reported considering the test structures in the no fire condition. Finally, mean elastic response spectra of acceleration for the NFE (Fig. 7(a)) and FFE (Fig. 7(b)) sets of earthquakes, assuming an equivalent

viscous damping ratio in the horizontal direction ( $\zeta_H$ ) equal to 5%, are compared with the corresponding target NTC08 design response spectrum at the CP limit state.

5. Numerical results

In order to evaluate the effectiveness of the base-isolation as a seismic retrofitting system of fire-damaged r.c. framed structures, the Nonlinear-Response-time History Analysis (NRHA) of the original (i.e., fixed-base) and retrofitted (i.e., base-isolated) buildings subjected to the horizontal components of the near-fault (i.e., set NFE) and

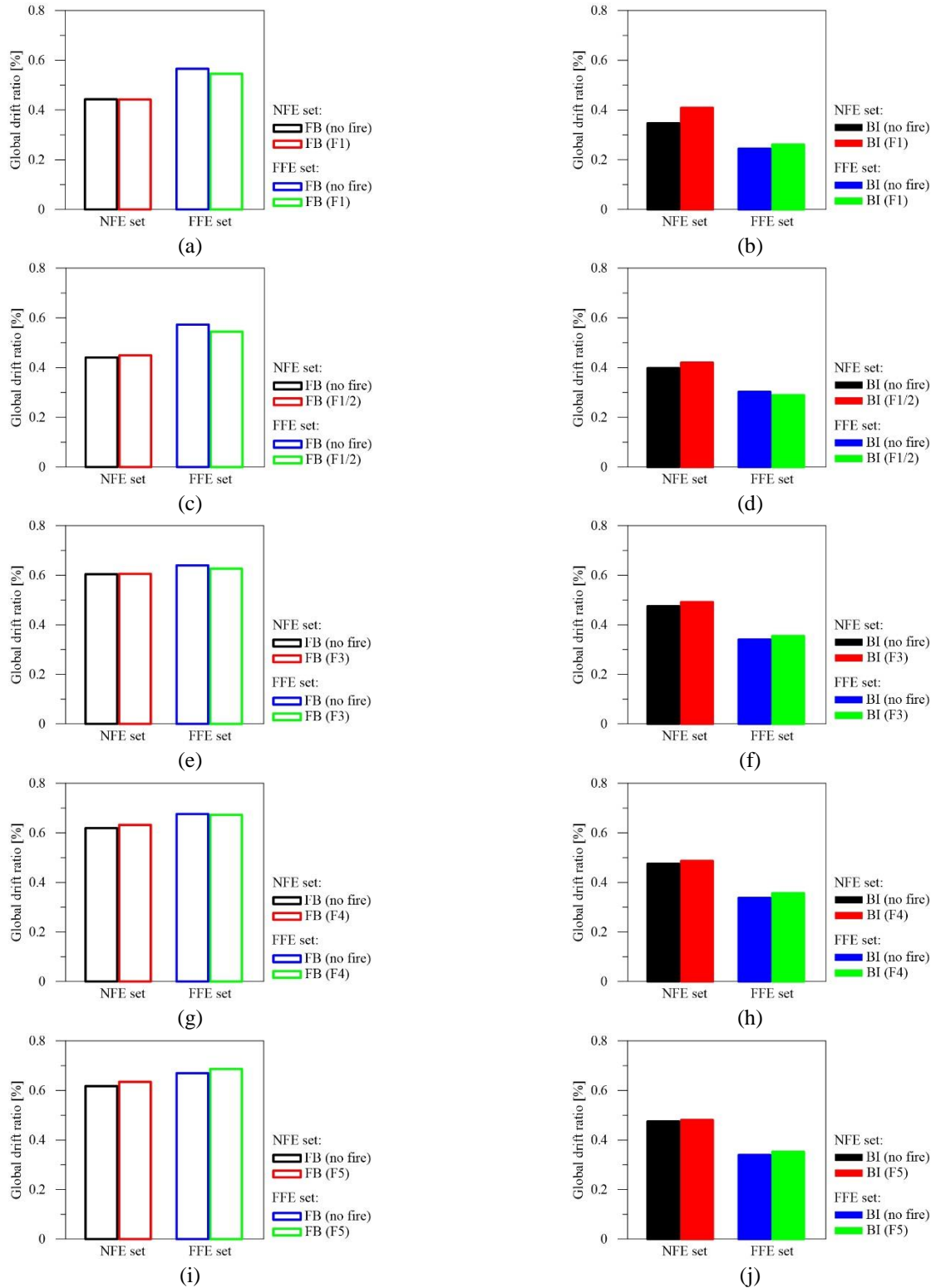


Fig. 8 Global response of the fixed-base (FB) and base-isolated (BI) fire-damaged structures subjected to the NFE and FFE sets of earthquakes

far-fault (i.e., set FFE) earthquakes is carried out. The results discussed below are obtained as an average of those separately obtained for each set of seven accelerograms, scaled to match the NTC08 response spectrum at the site where the structures are located. A lumped plasticity model based on the Haar-Kàrmàn principle describes the elastic-plastic response of the r.c. frame members (Mazza and Vulcano 2010), checking the ultimate ductility demand at the potential critical end sections of the beams and columns. Moreover, the viscous damping matrix of the superstructure is calculated on the basis of the Rayleigh damping. On the other hand, a two-spring-two-dashpot model with nonlinear force-displacement laws is adopted for modelling the coupling of horizontal and vertical responses for the HDLR bearings (Mazza and Vulcano 2012). The ultimate values of total and seismic shear strains of the HDLR bearings are assumed equal to 1.5 times the corresponding design values, while the compressive and tensile axial loads are limited to the critical buckling load and the ultimate tensile load, respectively.

In Fig. 8 the global structural damage of the superstructure is evaluated in terms of the maximum roof drift ratio, defined as the ratio of the peak horizontal roof displacement ( $u_{roof}$ ) to the building height ( $H_{tot}$ ). Note that horizontal displacement and height of the HDLR bearings are deducted from  $u_{roof}$  and  $H_{tot}$ , respectively, in the case of base-isolated structures.

In particular, original fixed-base (FB) and retrofitted base-isolated (BI) structures in the no-fire condition and at the end of 60 (i.e., R60) minutes of fire exposure are compared on the assumption that the fire compartment is confined to the area of the first level (i.e., F1, Figs. 8(a) and (b)), the first two levels (i.e., F1/2, Figs. 8(c) and (d)) and the other levels (i.e., Fi,  $i=1-3$ , Figs. 8(e)-(j)). In order to make the results comparable, the nonlinear dynamic analyses have been carried out assuming as final instant of simulation for each ground motion the minimum value from those first evaluated in both no-fire condition and selected fire scenario, also distinguishing different instants of time for the FB and BI structures. It is worth noting that, for all the examined cases, the NRHAs are interrupted once the ultimate value imposed on the ductility demand of the beams and/or columns at different floor levels has been reached. As can be observed, the global damage of the FB.F1 and FB.F1/2 structures subjected to the FFE set of earthquakes is greater than that for the same structures under the NFE set of motions (Figs. 8(a) and (c)), while only slight differences emerge when the Fi ( $i=3-5$ ) fire scenarios are considered. On the other hand, the BI structures have higher values of global damage for the NFE set than the FFE one. This behaviour can be explained by observing that the considerable increase in the deformability of a base-isolated structure, in comparison with that of the corresponding fixed-base structure, may lead to an amplification in the structural response under near-fault earthquakes. Finally, the results show that the retrofitted BI structures, where the base-isolation system is designed only for far-fault ground motions, always work better than the original FB structures also for the near-fault earthquakes.

Nevertheless, it is possible that FB or BI structures with similar values of the global drift ratio experience different levels of storey damage because a soft-storey mechanism is induced by local fire scenarios and/or near-fault ground motions. Therefore, the maximum storey drift ratio, defined as drift ( $\Delta$ ) normalized by the storey height ( $h$ ), is plotted in Fig. 9 for all storeys of the test structures. For a comparison, the results are also reported for the original fixed-base and retrofitted base-isolated structures in the no-fire condition. Moreover, the drift ratio thresholds related to different damage levels (i.e. repairable,  $\Delta/h \leq 0.5\%$ , irreparable,  $0.5\% < \Delta/h < 1\%$  and collapse,  $1\% \leq \Delta/h \leq 1.5\%$ ) of the r.c. frame members, in the case of nonductile structural systems, are represented (Ghobarah 2004). As shown, the fire-damaged FB structures suffer from moderately repairable to irreparable storey damage, with an amplification of the structural response localized to the level of the fire compartment (Figs. 9(a),(c),(e),(g) and (i)), while a slight reduction on the other levels in comparison with the no fire condition is generally obtained. For all fire scenarios, the effects of the NFE set on the drift ratio of the FB structures are found to be more marked at the lower storeys; on the contrary, drift ratios produced by the FFE set are generally more significant than those of the NFE set at the higher storeys, especially when the fire compartment is confined to these levels. As can be observed, the seismic retrofitting with a base-isolation system effectively reduces the drift ratio demand under the FFE set, generally falling within the light to moderately repairable range of damage (Figs. 9(b),(d),(f),(h) and (j)); while the pulse-type nature of the NFE set can induce unexpected drift ratios in the severe damage range, especially in the lower storeys. As expected, similar results are obtained for the base-isolated structures subjected to the FFE set when considering the no-fire condition and different fire scenarios. This happens because there is a considerable reduction of the horizontal seismic loads transmitted to the superstructure shifting the fundamental vibration period into the range of low spectral accelerations. However, an increase of drift demand of the BI structures occurs at the levels where the fire scenario is hypothesized, when the NFE set is considered.

Finally, to investigate the local structural damage of the fire-damaged buildings subjected to the NFE and FFE sets of earthquakes, maximum curvature ductility demand at the end sections of beams and columns is reported in Fig. 10. More specifically, the original (FB) and retrofitted (BI) fire-damaged structures are separately compared for each of the five fire scenarios.

Collapse of a fire-damaged r.c. framed building often occurs from the local concentration of deformation at the particular “weak-storey” exposed to fire or at the lower storeys under the NFE set of earthquakes. The effects of the FFE set on the ductility demand are found to be more marked for the FB.Fi structures than the BI.Fi ones, for all fire scenarios. Moreover, the effects of the FFE set are generally more significant than those of the NFE set at the higher floor levels of fixed-isolated structures, while the opposite is the case for the base-isolated structures.

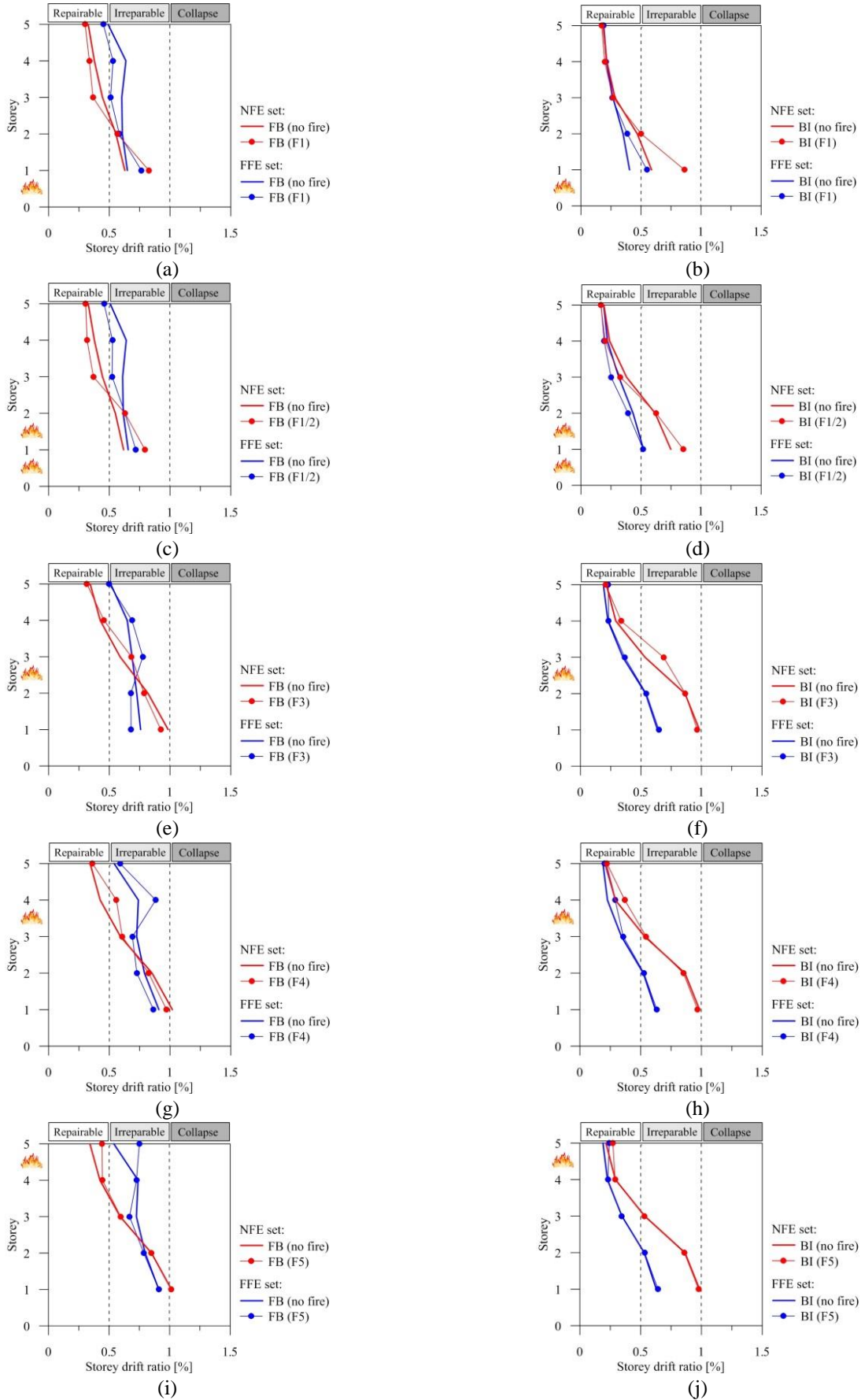


Fig. 9 Storey response of the fixed-base (FB) and base-isolated (BI) fire-damaged structures subjected to the NFE and FFE sets of earthquakes

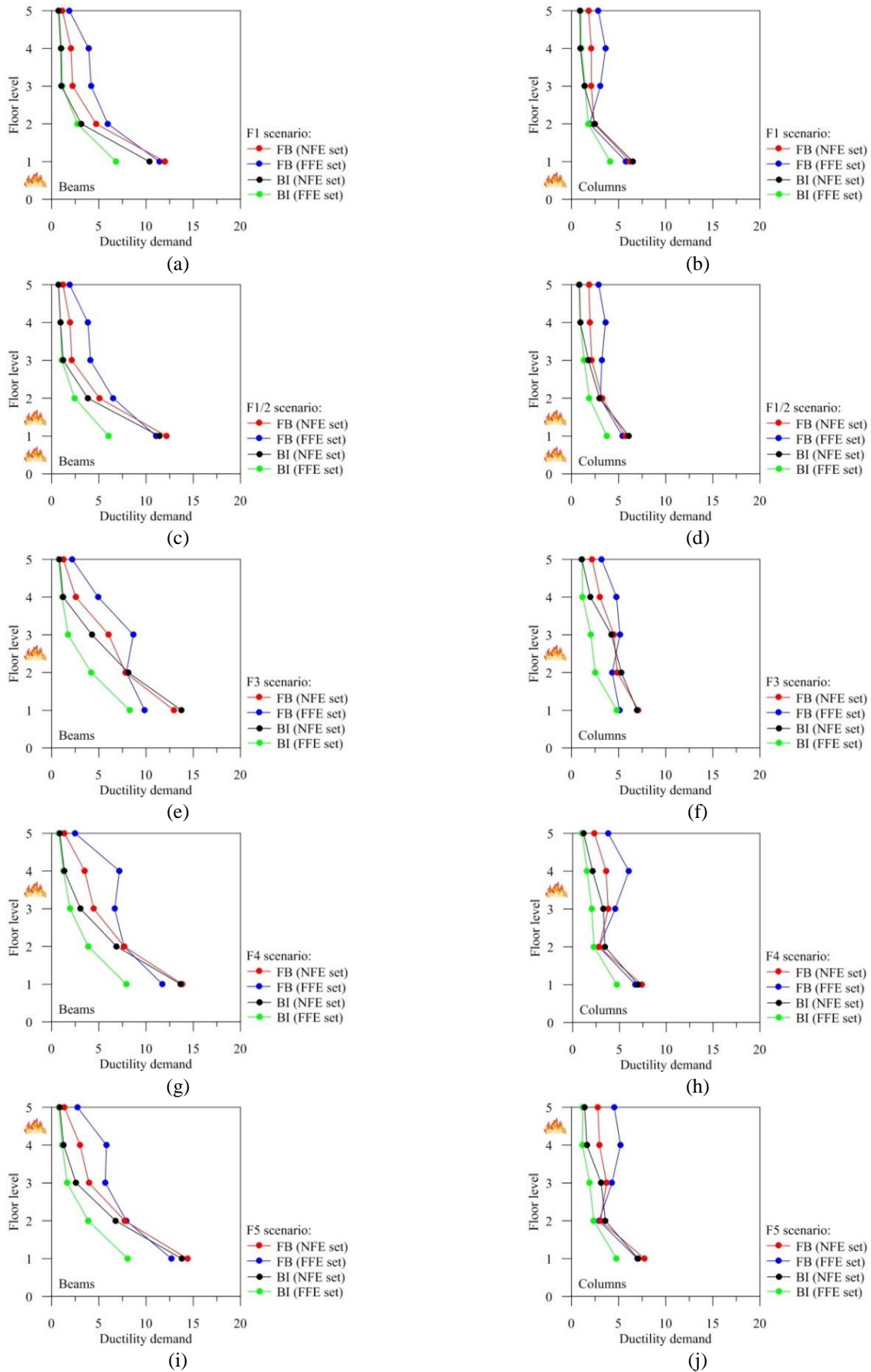


Fig. 10 Local response of beams and columns of the fixed-base (FB) and base-isolated (BI) fire-damaged structures subjected to the NFE and FFE sets of earthquakes

Further results, omitted for the sake of brevity, confirm seismic and total shear strains of the base-isolation system below their ultimate values under the NFE and FFE sets of earthquakes.

## 6. Conclusions

The work investigates the nonlinear dynamic response of fire-damaged r.c. framed buildings, designed as fixed-base in line with the former Italian code for a medium-risk seismic zone and then retrofitted with a base-isolation system to meet the requirements of the current Italian code in a high-risk seismic zone. Specifically, the original and retrofitted test structures are compared in the no fire situation and in the event of fire at the first level (F1), the first two (F1/2) and the upper (Fi,  $i=3-5$ ) levels of the superstructure considering 60 minutes of exposure.

Residual mechanical properties of fire-damaged r.c. frame members are preliminarily evaluated in accordance with the 500°C isotherm method proposed by Eurocode 2, carrying out thermal analysis of the cross-sections in line with the time-temperature curve of the fire compartments prescribed by Eurocode 1. Two sets of seven near-fault and far-fault earthquakes are selected from the American and European databases, respectively, selecting records with spectral shapes similar to the target design spectrum at the collapse prevention limit state. The following conclusions can be drawn from seismic results following fire.

The maximum global (roof) drift ratio of the FB.F1 and FB.F1/2 structures subjected to the FFE set is greater than that evaluated for the same structures under the NFE set, while only small differences are highlighted when the FB.Fi structures ( $i=3-5$ ) are considered. On the other hand, all BI structures show higher values of global damage under the NFE set than the FFE one, while their effectiveness in comparison with the original fire-damaged FB structures is always verified. In terms of the maximum local (storey) drift ratio, the fire damaged FB structures suffer moderately repairable and irreparable damage, with an amplification of the structural response in comparison with the no fire condition. In particular, damage is mainly concentrated at the level of the fire compartment and accompanied by a slight reduction on the other levels. The effects of the NFE set on the storey drift ratio of the FB structures are found to be more marked at the lower storeys; the opposite happens for storey drift ratios produced by the FFE set which are generally more significant than those of the NFE set at the higher storeys, especially when the fire compartment is confined to the area of these levels. The retrofitted BI structures effectively reduce the storey drift ratio under the FFE set, generally falling within the light to moderate repairable range of damage. The pulse-type nature of the NFE set can induce unexpectedly high values of the storey drift ratios, especially at the lower storeys of the BI structures. As expected, the retrofitted (base-isolated) test structures in the no fire situation and in the event of fire in the superstructure present similar results when subjected to the FFE set, while an increase of drift demand is obtained when considering the NFE set. Finally, local structural

damage, in terms of maximum ductility demand at the end sections of beams and columns, confirms that the FFE set is generally more significant than the NFE set at the higher floor levels of fixed-base structures, while the opposite happens for the base-isolated structures.

## Acknowledgments

The present work was financed by Re.L.U.I.S. (Italian network of university laboratories of earthquake engineering), in accordance with “Convenzione D.P.C.-Re.L.U.I.S. 2014-2016, WPI, Isolation and Dissipation”.

## References

- Baltzopoulos, G., Vamvatsikos, D. and Iervolino, I. (2016), “Analytical modelling of near-source pulse-like seismic demand for multi-linear backbone oscillators”, *Earthq. Eng. Struct. Dyn.*, **45**(11), 1797-1815.
- Bommer J.J. and Acevedo, A.B. (2004), “The use of real earthquake accelerograms as input to dynamic analysis”, *J. Earthq. Eng.*, **8**(1), 43-91.
- Bray, J.D., Rodriguez-Marek, A. and Gillie, J.L. (2009), “Design ground motions near active faults”, *Bull. NZ Soc. Earthq. Eng.*, **42**(1), 1-8.
- Dwaikat, M.B. and Kodur, V.K.R., (2009), “Hydrothermal model for predicting fire-induced spalling in concrete structural systems”, *Fire Saf. J.*, **44**, 425-434.
- ESD. European Strong Motion database. <http://esm.mi.ingv.it/>.
- Eurocode 1 (2004), *Actions on structures - Part 1-2: General actions, actions on structures exposed to fire*. C.E.N., European Committee for Standardization.
- Eurocode 2 (2004), *Design of concrete structures - Part 1-2: General rules, structural fire design*. C.E.N., European Committee for Standardization.
- Felicetti, R., Gambarova, P.G. and Meda A. (2009), “Residual behavior of steel rebars and R/C sections after a fire”, *Constr. Build. Mater.*, **23**(12), 3546-3555.
- Foti, D. (2015), “Local ground effects in near-field and far-field areas on seismically protected buildings”, *Soil Dyn. Earthq. Eng.*, **74**, 14-24.
- Ghobarah, A. (2004), “On drift limits associated with different damage levels”, *Proceedings of the International Workshop on the Performance-Based Seismic Design: Concepts and Implementation*, Bled, Slovenia.
- Gilmore, A.T. (2012), “Options for sustainable earthquake-resistant design of concrete and steel buildings”, *Earthq. Struct.*, **3**(6), 783-804.
- Italian Ministry of Public Works (1996), “Norme tecniche per le costruzioni in zone sismiche e relative istruzioni”, D.M. 16-01-1996 and C.M. 10-04-1997, n. 65/AA.GG..
- Iwan, W.D. (1997), “Drift spectrum: measure of demand for earthquake ground motions”, *J. Struct. Eng.*, **123**(4), 397-404.
- Lee, J., Xi, Y. and William, K. (2008), “Properties of concrete after high-temperature heating and cooling”, *ACI Mater. J.*, **105**, 334-341.
- Mazza, F. (2015a), “Seismic vulnerability and retrofitting by damped braces of fire-damaged r.c. framed buildings”, *Eng. Struct.*, **101**(15), 179-192.
- Mazza, F. (2015b), “Comparative study of the seismic response of RC framed buildings retrofitted using modern techniques”, *Eng. Struct.*, **9**(1), 29-48.
- Mazza, F. (2017), “Behaviour during seismic aftershocks of r.c.

- base-isolated framed structure with fire-induced damage”, *Eng. Struct.*, **140**(1), 458-472.
- Mazza, F. and Labernarda, R. (2017), “Structural and non-structural intensity measures for the assessment of base-isolated structures subjected to pulse-like near-fault earthquakes”, *Soil Dyn. Earthq. Eng.*, **96**, 115-127.
- Mazza, F. and Vulcano, A. (2010), “Nonlinear dynamic response of r.c. framed structures subjected to near-fault ground motions”, *Bull. Earthq. Eng.*, **8**(6), 1331-1350.
- Mazza, F. and Vulcano, A. (2012), “Effects of near-fault ground motions on the nonlinear dynamic response of base-isolated r.c. framed buildings”, *Earthq. Eng. Struct. Dyn.*, **41**(2), 211-232.
- Mollaioli, F., Lucchini, A., Cheng, Y., and Monti G. (2013), “Intensity measures for the seismic response prediction of base-isolated buildings”, *Bull. Earthq. Eng.*, **11**(5), 1841-1866.
- Mostafaei, H. (2013a), “Hybrid fire testing for assessing performance of structures in fire - Methodology”, *Fire Saf. J.*, **58**, 170-179.
- Mostafaei, H., (2013b), “Hybrid fire testing for assessing performance of structures in fire - Application”, *Fire Saf. J.*, **56**, 30-38.
- NTC08 (2008). *Technical Regulations for the Constructions. Italian Ministry of the Infrastructures*, D.M. 14-01-2008 and C.M. 2-2-2009.
- PEER. Pacific Earthquake Engineering Research Center database. <http://peer.berkeley.edu/smcat/search.html>.
- PROSAP. *PROfessional Structural Analysis Program*. Thermal analysis. Ferrara (Italy). <http://www.2si.it>.
- Somerville, P.G., Smith, N.F., Graves, R.W. and Abrahamson, N.A. (1997), “Modification of empirical strong motion attenuation relations to include the amplitude and duration effect of rupture directivity”, *Seismol. Res. Lett.*, **68**(1), 199-222.
- Sorace, S. and Terenzi G. (2014), “A viable base isolation strategy for the advanced seismic retrofit of an R/C building”, *Contemp. Eng. Sci.*, **7**(17-20), 817-834.
- Sorace, S. and Terenzi, G. (2015), “Seismic performance assessment and base-isolated floor protection of statues exhibited in museum halls”, *Bull. Earthq. Eng.*, **13**(6), 1873-1892.
- Tavakoli, H.R., Naghavi, F., Goltabar, A.R. (2015), “Effect of base isolation systems on increasing the resistance of structures subjected to progressive collapse”, *Earthq. Struct.*, **9**(3), 639-656.
- Youssef, M.A. and Mofteh, M. (2007), “General stress-strain relationship for concrete at elevated temperatures”, *Eng. Struct.*, **29**(10), 418-430.
- Zerbin, M. and Aprile, A. (2015), “Sustainable retrofit design of RC frames evaluated for different seismic demand”, *Eng. Struct.*, **9**(6), 1337-1353.

